Received: 29 September 2024 | Revised: 11 January 2025 | Accepted: 13 January 2025

DOI: 10.1002/mp.17708

RESEARCH ARTICLE

MEDICAL PHYSICS

Demonstration of virtual imaging trial applications for optimization and education of dento-maxillofacial CBCT imaging

Karen Merken[1] | **Nicholas Marshall**[1] | **Johan Nuyts**[2] | **Rodrigo T Massera**[1] | **Reinhilde Jacobs**[3,4] | **Hilde Bosmans**[1]

[1]KU Leuven, Department of Imaging and Pathology, Division of Medical Physics & Quality Assessment, Leuven, Belgium

[2]KU Leuven, Department of Imaging and Pathology, Division of Nuclear Medicine & Molecular Imaging, Leuven, Belgium

[3]KU Leuven, Department of Imaging and Pathology, Division of Oral and Maxillofacial Surgery, Leuven, Belgium

[4]Department of Dental Medicine, Karolinska Institute, Stockholm, Sweden

Correspondence
Hilde Bosmans, KU Leuven, Department of Imaging and Pathology, Division of Medical Physics, and Quality Assessment, Leuven, Belgium.
Email: hilde.bosmans@uzleuven.be

Funding information
Katholieke Universiteit Leuven, Grant/Award Number: C24/18/065; Research Foundation Flanders; Flemish Government

Abstract

Background: A number of studies have suggested that there is a need for improved understanding of dento-maxillofacial cone beam computed tomography (CBCT) technology, and to establish optimized imaging protocols. While several ex vivo/in vitro studies, along with a few in vivo studies, have addressed this topic, virtual imaging trials could form a powerful alternative but have not yet been introduced within the field of dento-maxillofacial imaging.

Purpose: To introduce and illustrate the potential of utilizing a virtual imaging trial (VIT) platform for dento-maxillofacial CBCT imaging through a number of case studies.

Methods: A framework developed in-house, simulating an existing CBCT scanner, and the necessary digital patient phantoms were prepared for the following potential studies: I) the impact of intracanal material type (Ni-Cr alloy, fiberglass, gutta-percha) and acquisition settings (tube current (mA), tube voltage (kVp)) on root fracture (RF) visibility; II) image artefact levels from candidate new restorative materials, such as graphene; III) the effect of patient rigid motion on image artifacts; IV) the effect of a metal artifact reduction algorithm on RF visibility in a tooth treated endodontically and restored with a metal post. In addition, features not available on the real system, including automatic exposure control and extended tube current and tube voltage ranges, were added to study the impact of these parameters. Patient dose levels were also quantified.

Results: The generated images showed the influence of different restorative materials, dose levels, rigid motion, and image processing on the quality of the final images. Results of these simulated conditions were consistent with findings in the literature. Patient effective dose levels ranged between 22 and 138 μSv for all simulated scenarios. Images were considered sufficiently realistic according to an experienced oral radiologist. Furthermore, the platform was able to simulate scenarios that are difficult or impossible to replicate physically in a controlled and repeatable way.

Conclusions: A virtual imaging trial platform has the potential to improve the understanding and use of CBCT technology. Improved insight into system performance can lead to optimized imaging protocols, and help to reduce the large variation in system setup and performance currently seen in clinical practice in dento-maxillofacial CBCT imaging.

KEYWORDS
clinical applications, dento-maxillofacial CBCT imaging, system optimization and education, virtual imaging trials

1 | INTRODUCTION

In many countries, dental exposures make up a significant contribution to the overall number of medical x-ray imaging acquisitions. The most commonly performed radiological examinations are 2D imaging techniques, such as intraoral and extraoral panoramic and cephalometric radiography.[1] However, over the past two decades, the use of cone beam computed tomography (CBCT) imaging has become increasingly popular for diagnosis and treatment planning.[2] Currently, there exist many different models that often operate under a broad range of imaging protocols, leading to a wide variation in imaging performance.[2,3] This suggests that improving the understanding of CBCT technology could help to establish optimized imaging protocols in the future.[4,5]

System optimization via clinical trials is generally not feasible for a number of reasons, including cost, the need for ethics clearance, and a lack of ground truth.[6] In addition, in real patients, the dose to the organs cannot be assessed in vivo.[6] Alternatively, ex vivo/in vitro studies using anthropomorphic phantoms are frequently performed in dento-maxillofacial imaging research.[7] These types of studies are subject to significantly fewer ethical constraints, and the ground truth can be known. However, although representing realistic anatomy, these studies are time-consuming and struggle to capture all the nuances of real tissue x-ray attenuation.[8] Furthermore, all of the methods discussed require long periods of scanning, while the clinical workflow often limits access to a system. In addition, only the scan protocols or technologies available on the commercial scanners can be studied.

In recent years, the use of computer simulations that model the complete x-ray examination, that is, the patient with a specific pathology, the x-ray imaging system, and the radiologist, has been gaining popularity.[4,6] Provided that these computational models are sufficiently realistic, many of the difficulties mentioned above can be avoided. Therefore, simulation is considered to be a promising alternative to clinical trials, in what is referred to as virtual imaging trials (VITs). This technique allows the investigation of the impact of imaging parameters on system performance in a controlled environment where the ground truth is exactly known. In addition, the potential of new pre-clinical technologies can be assessed, and patient organ doses can be obtained in parallel as well.[6]

In magnetic resonance imaging (MRI) and computed tomography (CT) imaging, the use of these virtual simulation platforms, not only as a tool for optimization, but also for the education of medical personnel, has been proposed in the literature.[5,6,9–11] However, the use of VITs has not yet been described for dento-maxillofacial imaging. Given the potential of this type of tool in education and system optimization, the aim of this work is to introduce and illustrate a VIT platform for dento-maxillofacial CBCT applications through a number of case studies.

2 | METHODS

2.1 | Virtual platform

VIT methods anticipate a fully virtual simulation chain, from patient and imaging task, through a virtual CBCT system, leading to interpretation by a computational observer. The scenes and clinical tasks generated by the VIT platform described in this work are complex, and computational observer methods are not yet available to perform virtual image interpretation. Human observers were therefore used to read, interpret, and evaluate the generated image content.

2.1.1 | Virtual patient

A multiresolution adult head voxel phantom, consisting of 0.05 mm high-resolution tooth models that can be inserted into a lower resolution head phantom of 0.2 mm, served as a virtual patient. The model was previously developed for image quality optimization studies in dento-maxillofacial CBCT imaging.[4] The normal anatomy of the virtual patient model was based on segmentations from clinical CBCT scans. To simulate a selection of clinically relevant tasks, detailed models of root fractures (RFs) and dental restorations (implants, fillings, and root canal treatments (RCTs)) were developed and can be inserted into the phantom in any desired configuration. Figure 1 shows an overview of the developed model, including the normal anatomy with the dental structures visualized in detail, and examples of the modeled clinical tasks. As detailed dosimetry is not yet possible using this phantom, the models developed by Stratis et al.[12] were used to estimate the effective dose level to the patient. In this study, a database of pediatric voxel models ranging from a 2-month-old baby to a 14-year-old patient was created specifically for dosimetry applications in dento-maxillofacial imaging. Given that the circumference of the head generally does not experience significant growth after the age of 14,[13] in

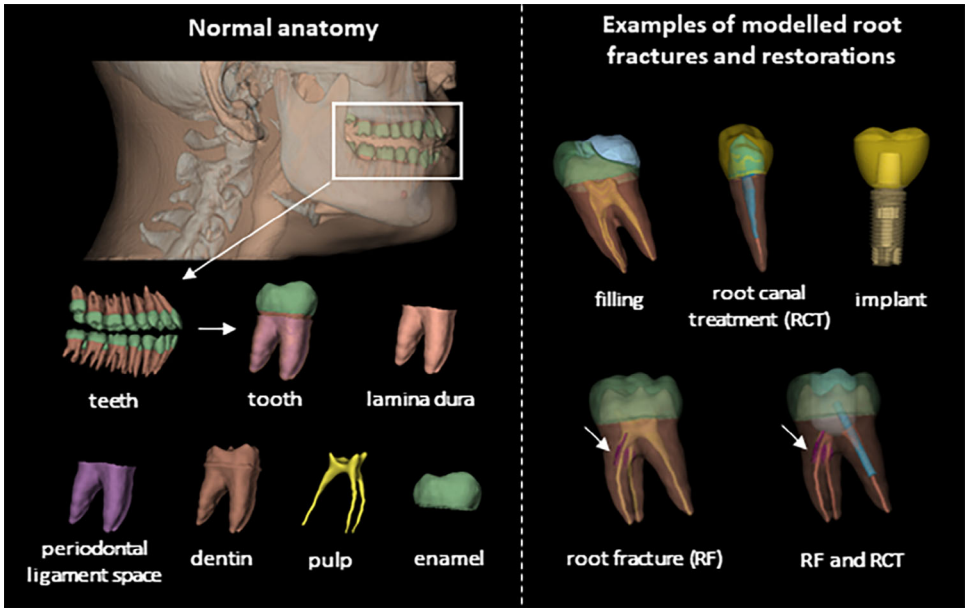

FIGURE 1 Overview of the developed patient model.

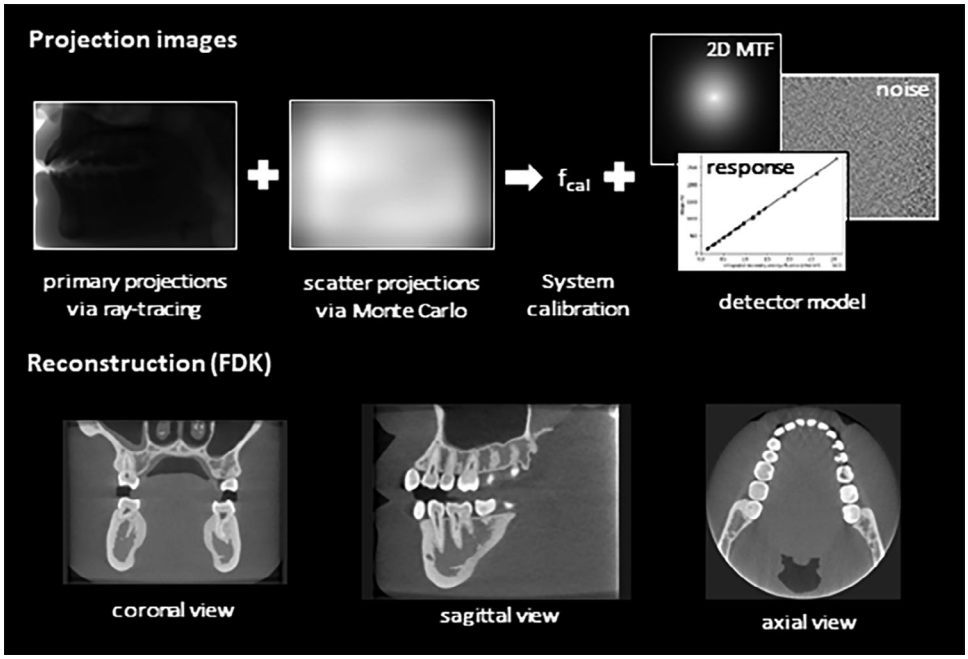

FIGURE 2 Overview of the image simulation chain.

this study, the 14 year old model was used to estimate the adult patient dose.

2.1.2 | Virtual acquisition

Image simulation

Image simulation was performed using an in-house simulation framework for dento-maxillofacial CBCT imaging, developed and validated by Merken et al.[14] Figure 2 gives an overview of the image simulation chain, which consists of four parts: the x-ray source, the rotational projection, the detector, and the image reconstruction. A 3D Accuitomo 170 (Morita, Japan) system was modeled. In summary, the x-ray source was characterized by the energy spectrum and experimentally determined weighting factors reflecting the attenuation of the inherent fixed bowtie-like filtration. Primary projections were

generated via ray-tracing, while Monte Carlo simulations were used to estimate the scattered radiation. System calibration, as well as the modeling of the detector energy response function, and realistic levels of image noise and blurring, were based on experimental measurements from the real system. Images were reconstructed using the FDK (Feldkamp, Davis and Kress) algorithm for filtered backprojection CBCT image reconstruction.

For this study, images were simulated using the acquisition parameters as specified on the real system associated with the standard operation mode for small to medium field of view (FOV) size settings: an acquisition time of 17.5 s, a detector read-out speed of 30 frames per second, 512 image frames per rotation, a source-object-distance of 54 cm, a source-detector-distance of 84.2 cm, and a detector pixel size of 0.254 $\times$ 0.254 mm^2.[14] All of these and the remaining system parameters that were needed for system modeling can also be found in ref. [14]. Since both the ray-tracing and MC software can only handle single-resolution models, a specific simulation strategy, as described by Merken et al.,[4] was used to deal with the multiresolution nature of the image quality phantom. In this approach, the primary projection images were determined separately for the high-resolution tooth models and for the remaining lower resolution structures, and then combined into a single simulated CBCT acquisition. Scattered radiation was estimated based on simulations of a lower resolution version of the complete phantom.

Effective dose calculation

Patient organ dose levels were obtained by employing the Monte Carlo part (PENELOPE/penEasy software[15]) of the framework. Application of the ICRP 103 tissue weighting factors then resulted in the patient effective dose level.[16] The voxel models developed by Stratis et al.[12] consist of 22 organs, but exclude the red bone marrow (RBM) and the lymph nodes.

The dose to the lymph nodes was therefore estimated as a weighted sum over the doses in surrogate organs, following the same approach as defined for PCXMC, and including only the organs relevant for dento-maxillofacial imaging,[17]

$$D_{\text{lymph}} = 0.13D_{\text{ET}} + 0.08D_{\text{salivary glands}} + 0.05D_{\text{thyroid}} + 0.04D_{\text{esophagus}} + 0.05D_{\text{total body}} \quad (1)$$

with D is the absorbed organ dose in each of the respective organs, and ET referring to the extrathoracic region.

The RBM is located in small cavities in the trabecular bone. In the models, the trabecular bone and the cortical bone were segmented as a uniform skeletal mixture.[18] The dose to the RBM was then estimated from the dose deposited to the skeletal mixture by applying correction factors,[19–21]

$$D_{\text{RBM}} = \sum_{i=1}^{N_E} D_{\text{Bone}}(E_i).\frac{\left(\frac{\mu_{en}(E_i)}{\rho}\right)_{\text{RBM}}}{\left(\frac{\mu_{en}(E_i)}{\rho}\right)_{\text{Bone}}} \cdot S(E_i) \quad (2)$$

with N_E the number of energy bins, $\mu_{en}(E)/\rho$ the mass-energy absorption coefficients of the respective organs, and $S(E)$ the dose intensification factor.[19] The RBM dose was then subtracted from the total bone dose to obtain the correct dose to the surrounding bone tissue. In order to calculate the dose to the RBM as specified in Equation (2), an adapted version of the PENELOPE/penEasy energy deposition tally had to be used.[22]

For organs only partially located inside the head, the organ dose was multiplied by the segmented fraction of the total mass of the organ in the entire body. Simulations were run until the relative statistical uncertainty on the dose estimations was less than 1 %.

2.2 | Applications

In this section, possible applications of the developed platform are illustrated by means of four case studies. All the simulations were performed using supercomputing resources (KU Leuven VSC, Genius Tier-2 cluster). Intel Cascade Lake thin nodes with 192 GB RAM were used, each consisting of 2 Xeon Gold 6240 CPUs @ 2.6 GHz containing 18 cores each.

Case study I

Currently, one of the most challenging tasks for dental professionals in daily practice is a definitive diagnosis of RFs.[7,23] This is because RFs predominantly occur in endodontically treated teeth, that is, after RCT. The intracanal materials, filling the root of the tooth, used during this type of treatment are often dense in nature, generating artifacts, which can lead to a misdiagnosis.[23,24]

The virtual platform can be used to study the influence of different imaging parameters on RF detection in a controlled way. This case study illustrated, the impact of intracanal material type and acquisition parameter settings on RF visibility. A RCT task was modeled in a lower jaw first molar, along with a RF with a maximum width of ~0.25 mm in the axial image view. Four different intracanal materials were simulated: pulp, fiberglass, gutta-percha, and Ni-Cr alloy. Material compositions and densities were taken from the literature and manufacturer safety data sheets. The pulp case represented the reference scenario.

Regarding the simulated acquisition parameters, both the tube current (mA) and the tube voltage (kVp) were varied: images were simulated at 90 kVp and 5 mA,

which is the standard clinical setting, and at 90 kVp and a three times higher tube current of 15 mA. Images were also simulated at 75 and 120 kVp tube voltage. For each of these tube voltages, a new system calibration factor, required to relate the simulated number of photons to the number of photons in a real acquisition and expressed in photons/mAs, had to be determined. For the 75 kVp setting, the approach described by Merken et al.[14] for the standard clinical tube voltage of 90 kVp was repeated. To calibrate the system to simulate images at 120 kVp, a setting not available on the real system, the calibration factor was estimated; an approximation for the measured detector air kerma (DAK) per tube current-exposure time product (in μGy/mAs) was obtained by measuring the DAK between 60 and 90 kVp, which covers the available tube voltage range on the system. Steps of 10 kVp at settings of 0.033, 0.12, 0.17, 0.25, and 0.33 mAs/projection were used. A power relationship was then fitted to DAK per tube current-exposure time product as a function of tube voltage and the value at 120 kVp was extrapolated. The tube current level used for the generation of images for the two additional tube voltages was determined from additional simulations, using a technique similar to the operation of an automatic exposure control (AEC) system. To do this, the tube current was similar to the DAK measured at the standard clinical setting (90 kVp, 5 mA) for the posterior-anterior and lateral views. These two views correspond to the most and least attenuating views, respectively, and are typically used as scout views for patient positioning. A 4×4 cm^2 FOV, with a reconstructed voxel size of 0.08 mm was selected. A Hann reconstruction window was applied. In addition, for each of the four simulated acquisition protocols, the effective dose to the patient was calculated.

Case study II

In dentistry, the development of new materials used for patient treatment is an active area of research. Currently, there is a growing interest in graphene-based nanocomposites, especially in implant dentistry for use as potential crown material.[25] From a radiological point of view, graphene has the potential to reduce the severity of artifacts compared to the very dense restorative materials commonly used today.[26]

In this example, the virtual platform was used to study the effect of implant crown material on image artifacts. A lower jaw molar was replaced with an implant model. Two crown materials were simulated: the commonly used zirconia, and a more recent graphene-based material, that is, PLA/HA/GO nanocomposite.[26] For the implant and abutment, titanium was used. Images were simulated at the standard clinical setting of 90 kVp and 5 mA. A FOV size of 11×8 cm^2, with a reconstructed voxel size of 0.2 mm and a Hann reconstruction window, was selected. An estimate of the patient effective dose level was also determined.

Case study III

In addition to the presence of very dense restorative materials, patient motion is one of the most common causes of image artifacts in dento-maxillofacial CBCT imaging. As with metal streak artifacts, motion affects image quality, and may negatively impact diagnosis.[27,28].

This third case study illustrates the influence of patient rigid motion on image artifacts, with and without the presence of additional metal streak artifacts. Rigid patient motion in the form of a small rotation of the head was used to study motion artifacts. To do this, a rotation of $\sim$10° over a period of 2 s during the full rotation (17.5 s) was simulated. The patient model from case study II containing the zirconia crown was used. Simulations were performed at the standard clinical setting using an 11×8 cm^2 FOV, with a reconstructed voxel size of 0.2 mm. A Hann reconstruction window was applied.

Case study IV

Different types of reconstruction and post-processing algorithms have been developed and are subject to continuous development.[27,29–31] These algorithms can influence the quality of the final images and should be optimized for the clinical imaging protocols used. In this final case study, the impact of a metal artifact reduction (MAR) algorithm on image artifacts and RF visibility was simulated. A RCT, with a cast post, was modeled in the first premolar of the lower jaw, together with an RF with a maximum width of $\sim$0.25 mm in the axial image view. Simulations were performed with a pulp, that is, the reference and a Ni-Cr alloy cast post. The simulated crown material was zirconia. A simple projection completion MAR algorithm, using linear interpolation to replace the metal values in the sinogram, was then applied to the image with the Ni-Cr alloy post.[32] Images were simulated at the standard clinical setting of 90 kVp and 5 mA, and using a 4×4 cm^2 FOV, with a reconstructed isotropic voxel size of 0.08 mm. A Hann reconstruction window was applied, and the patient effective dose level was calculated.

3 | RESULTS

3.1 | Applications

Case study I

Figure 3 depicts the DAK per tube current-exposure time product, measured as a function of tube voltage, together with the fit curve needed to describe the system at 120 kVp. Radiation output is approximately proportional to the square of the tube voltage. Resulting calibration factors and tube current levels were 3.88e^{10} photons/mAs and 11 mA, and 1.21e^{11} photons/mAs and 1.6 mA for, respectively the 75 and 120 kVp simulations.

Figure 4 shows axial views of the restored molar in the resulting images of the first case study. For all

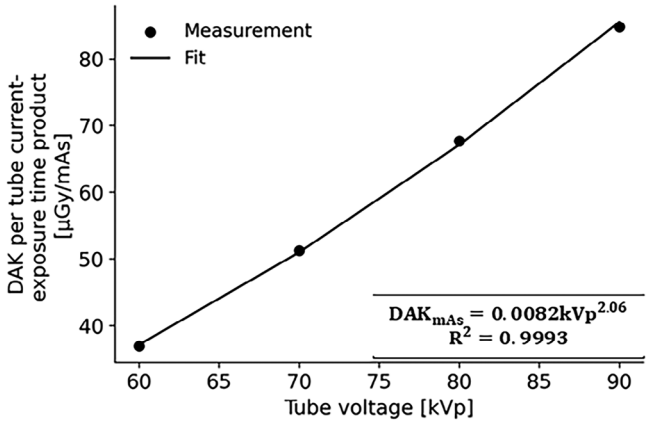

FIGURE 3 The DAK per tube current-exposure time product (DAK_{mAs}), measured as a function of tube voltage (kVp). DAK, detector air kerma.

TABLE 1 Effective dose levels for the simulated system settings.

Tube voltage (kVp)	Tube current (mA)	Effective dose (μSv)
90	5	30
90	15	90
75	11	38
120	1.6	22

the modeled scenarios, differences in RF visibility were observed between the fiberglass and the gutta-percha and the Ni-Cr alloy cases. RF visibility for the fiberglass material was similar to that for the pulp case (reference). Increasing the dose level for the 90 kVp case made the RF more apparent compared to the standard clinical setting for the reference and the fiberglass cases. For the gutta-percha and Ni-Cr alloy, increasing the dose level did not give an obvious improvement in RF visibility. The blooming artifact was observed for the gutta-percha and Ni-Cr alloy cases. Regarding the images simulated at 75 and 120 kVp, using the AEC approach, the noise level was similar to that for the standard acquisition protocol. This is only approximate as an exact match between noise values would require identical energy fluence levels at the detector input. In addition, for the gutta-percha and Ni-Cr alloy case, artifacts were respectively slightly more and less pronounced at 75 and 120 kVp. The applied change in tube voltage did not have a large effect on RF visibility. Table 1 gives the calculated patient effective dose levels for each of the simulated settings. For the AEC approach, effective dose levels decrease with increasing tube voltage. Although the depth of interaction and energy deposition to the internal organs increases as energy is increased, this is counterbalanced by a reduction in overall milliampere-seconds required to reach the target DAK. The reduction in milliampere-seconds results from the increased penetration through the patient as tube voltage increases.

Case study II

Figure 5 shows axial and sagittal views of the resulting images of the second case study. A clear reduction in artifacts was observed for the PLA/HA/GO implant crown compared to the zirconia case. The reduction was visible throughout the whole image; at further distances from the implant, but also in the vicinity of the implant, the adjacent teeth were less affected when the graphene-based crown was used. Enlarged image views of the proximity of the implant in Figure 5 are included for clarity. The patient effective dose was 138 μSv.

Case study III

Figure 6 shows axial views of the resulting images of the third case study. To demonstrate the impact of motion without and with additional metal streak artifacts, an image slice from the upper and lower jaw were selected, respectively. Obvious image artifacts were induced by the simulated motion, which seemed to be enhanced by the presence of the zirconia crown. The patient effective dose was the same as for case study II.

Case study IV

Figure 7 shows axial and sagittal views of the resulting images of the fourth case study. Axial views are shown at the level of the crown as well as the RF. The sagittal view is shown at the RF level. The application of the MAR algorithm clearly reduced the degree of artifacts in the image. For this specific scenario, the RF was not visible independent of the application of the MAR. For this simulated scenario, the patient effective dose level was 25 μSv.

4 | DISCUSSION

This work demonstrated the use of a VIT platform as a potential tool for teaching and optimization of dento-maxillofacial CBCT imaging performance. The main application has currently focused on studying the effect of different imaging parameters on image artifacts and RF visibility.

It should be noted that the aim of this work was to illustrate the potential and possible benefits of the virtual imaging method for some aspects of dento-maxillofacial CBCT imaging. A full study would be required to quantify the influence of the different parameters on RF detectability and on image artifacts.

The first case study illustrated the impact of different intracanal materials and acquisition parameters on RF visibility. Although CBCT imaging has clear potential for studying RF diagnosis, there is still no current consensus on the accuracy of this method. As a consequence,

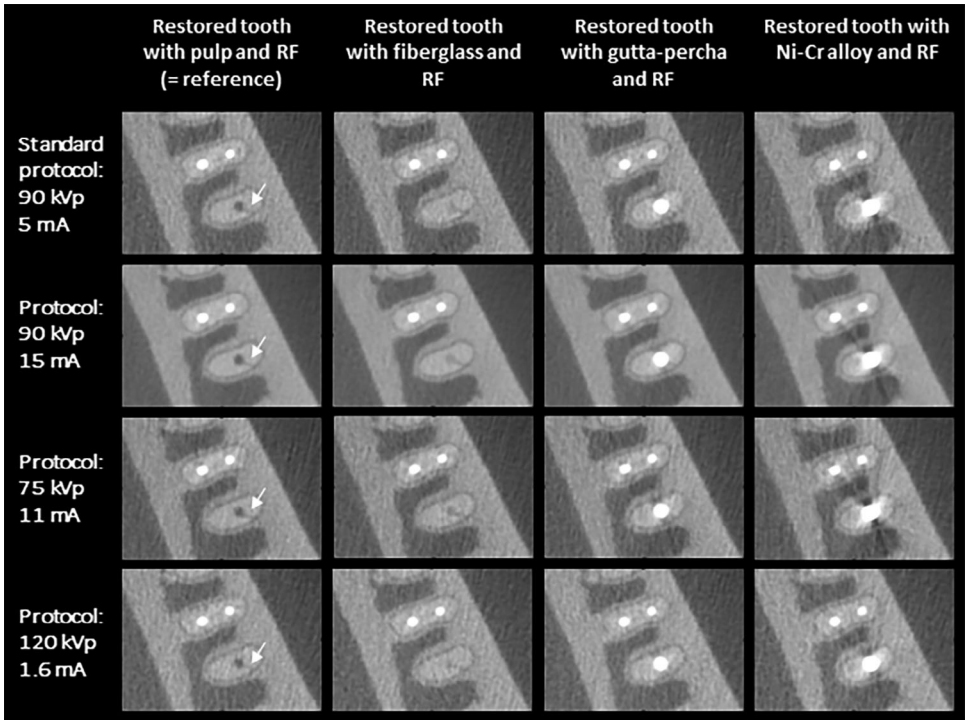

FIGURE 4 Axial views of the resulting images for all the simulated scenarios in case study I. Only image crops around the restored molar are shown. The arrow indicates the location of the RF in the reference case. RF, root fracture.

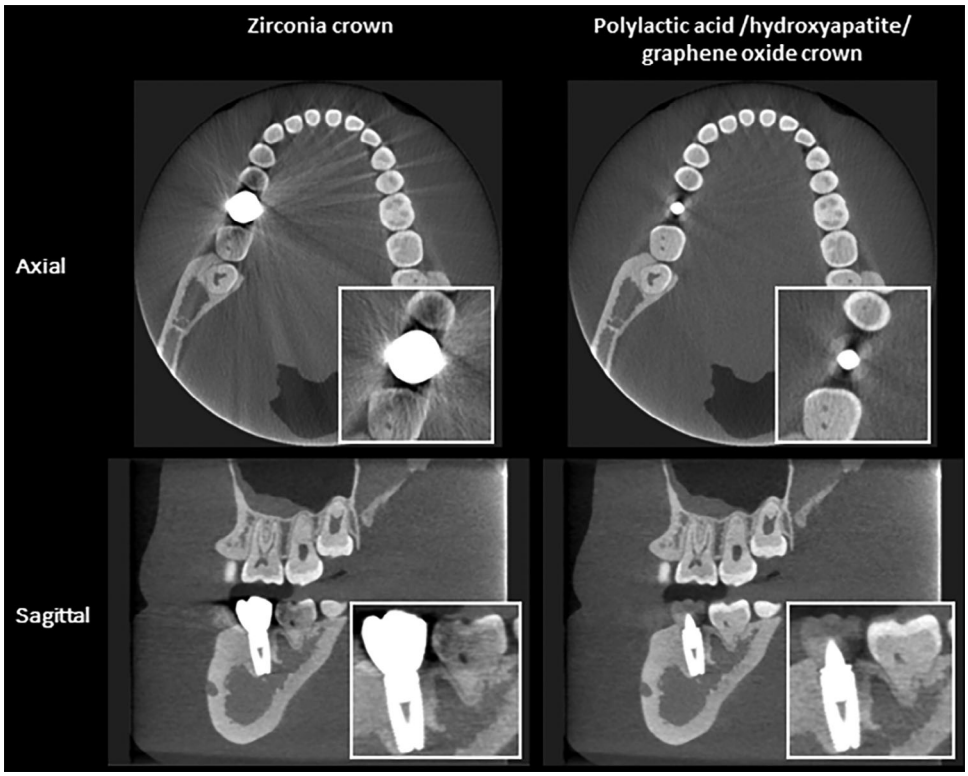

FIGURE 5 Axial and sagittal views of the resulting images for the simulated scenarios in case study II. Enlarged views of the implant crown are also shown for each case.

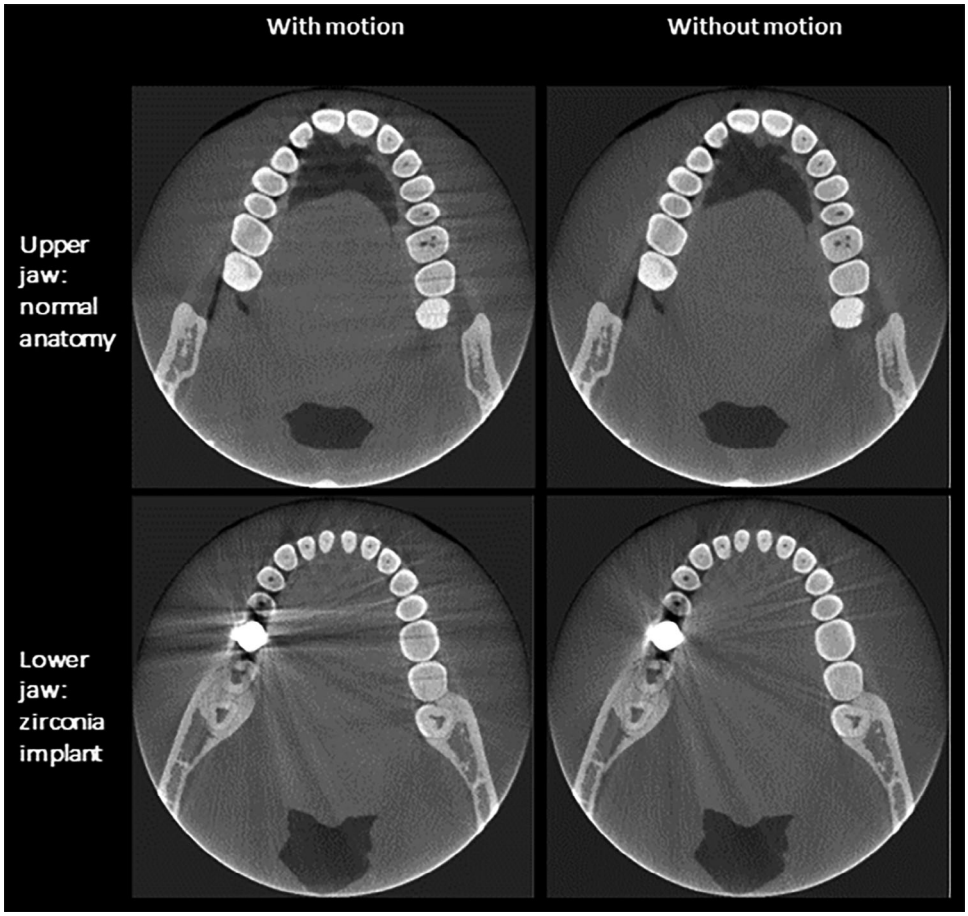

FIGURE 6 Axial views of the simulated scenarios in case study III.

various studies have been performed to address this problem, most of which are ex vivo or in vitro studies, with only a few in vivo studies.[7] The results here showed that similar findings can be obtained via simulation and therefore provide an alternative.

Although only one very specific clinical scenario was simulated, qualitatively, the observations were found to be consistent with the results reported in literature.[8,33,34] It should be emphasized that once the models were developed, similar simulations could be generated relatively quickly. In addition, exactly the same tooth was easily simulated with different types of materials, with and without pathology, providing paired observations. While often not possible clinically, paired studies can potentially reduce the required sample size, and consequently limit the number of images required to be read by human observers in order to reach reliable conclusions. Patient position in the simulation was known exactly, obviating the need for co-registration of images from different acquisitions. Moreover, system parameters could be varied independently of each other, something that is usually not feasible on real systems, where parameters often have a limited range or have fixed values for given acquisition programs. In the simulated case study, both the tube current and tube voltage levels were increased over larger ranges compared to those available on the real system. While the real system has no AEC functionality, a means of implementing an AEC was directly examined using the simulation platform. This allowed acquisition parameters to be varied in a more controlled way. Using a simple AEC method to set the tube current for a different tube voltage level resulted in similar image noise levels for the new tube voltage and for the standard clinical setting, enabling the effect of a change in x-ray spectrum to be studied independently of the image noise level. On the real system, this would not be possible without a similar test object (matching the virtual head phantom) and measurement equipment. Furthermore, the exact tube current setting needed to set this dose level may not be physically available on the system. Finally, the effective dose to the patient could be determined in parallel. This allows complete optimization studies to be performed in the future, balancing patient radiation dose and image quality for a specific clinical indication.

The second case study illustrates the image artifact suppression ability of graphene, a new material that has potential use in dental implantology. As graphene is not

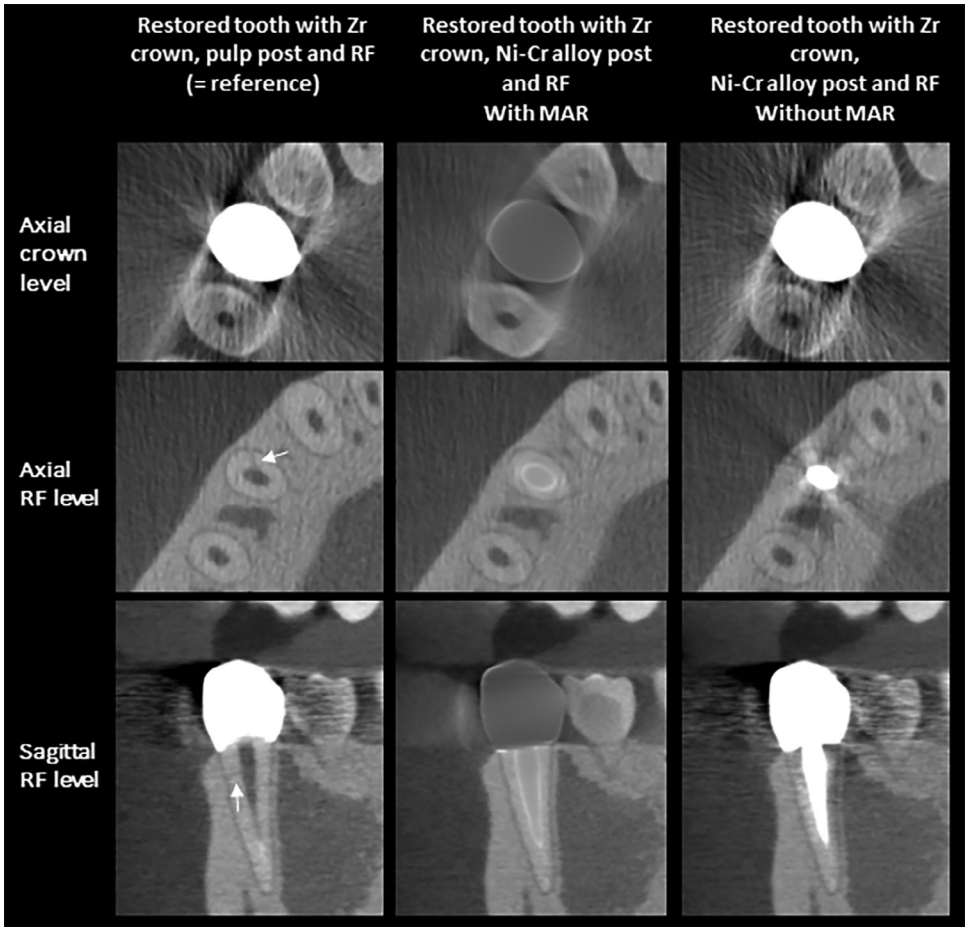

FIGURE 7 Axial (at crown and RF level), and sagittal (at RF level) views of the resulting images for the simulated scenarios in case study IV. Only image crops around the restored premolar are shown. RF, root fracture.

yet widely utilized in clinical practice, obtaining graphene samples or, more importantly, graphene-based implant models is not straightforward; in ref. [26], for example, cylindrical objects were used to study the effect of the PLA/HA/GO composite on image artifacts. The images produced using the simulation framework were consistent with the results of that study.[26] However, the virtual imaging platform had the potential to implement realistic patient scenarios and consequently perform more complex studies. For example, scenarios including various implant positions in combination with different pathologies, such as RFs or caries[35,36] could be examined. This would offer a means of investigating the full impact, from a radiological point of view, of new candidate dental materials.

The third case study showed the effect of rigid motion on image artifacts. Although patient motion is a major cause of image degradation in dentomaxillofacial CBCT imaging, only a limited number of studies have examined the effect of motion on diagnostic performance.[28] One reason for this may be that investigating patient motion in a controlled or repeatable manner on real systems is not straightforward, requiring the simulation of different types of motion, with specific direction, rotation, duration, and timing. It is clearly unacceptable to ask patients to move explicitly during a scan. Even using virtual techniques, simulation of patient motion remains challenging, and the existing patient model should be extended to include nonrigid patient motion to increase clinical relevance. Nevertheless, the use of virtual techniques to produce patient motion allows full control over all the aspects of the movement, that is, direction, rotation, duration, acceleration, and so forth. Furthermore, simulated motion is exactly reproducible. The same patient model could be scanned with and without motion, with or without the presence of pathologies or dental restorations. This allows the study of patient motion in a controlled and repeatable way, something that is more challenging in a real trial.

The fourth and last case study showed that the simulation platform can be used to assess the impact of image processing techniques on diagnostic performance. In this work, a specific MAR algorithm was stud-

ied. Although other types of MAR algorithms exist,[37,38] the result observed in this study was similar to findings in the literature.[34,36] One possible application of the framework is in the comparison of different commercially available MAR algorithms. These could be applied to the same input simulations, allowing like-for-like comparisons of algorithms for a range of clinical conditions. Simulations can be used to test newly developed algorithms, including post-processing and image reconstruction methods, in terms of clinical task performance. While real experimental or clinical studies are possible, appropriate test objects reflecting a realistic patient are required but not easily available. Studies using real patients on the other hand have the advantage of realism; however, the exact pathological condition, that is, the ground truth of a given case is usually not known.

The case studies presented in this work have illustrated the potential use of a virtual platform as a tool for teaching and optimization in dento-maxillofacial CBCT applications, both for researchers and clinical personnel. Although promising, the current model has some limitations. Regarding the patient model,[4] detailed modeling of trabecular bone structure remains the subject of future work, and will increase the range of pathologies that can be studied. Currently, only rigid motion can be simulated, while the addition of non-rigid motion, for example, swallowing and tongue motion would improve the realism level as well as the clinical relevance. Future work will also extend phantom development to include pediatric cases and multiple models that can represent the anatomical variability present in the clinical population. Regarding system modeling, the potential of new technologies, such as dual energy or photon counting detectors in dento-maxillofacial CBCT applications can be explored. If detailed system measurements can be made on scanners from different vendors then a performance comparison can be made using the same dataset of simulated imaging tasks. It is believed that maintaining, updating, and applying a virtual imaging platform can lead to the optimized use of dento-maxillofacial CBCT in future clinical practice.

5 | CONCLUSIONS

This work has described four case studies using a dento-maxillofacial CBCT system simulation platform. Current applications include the study of different imaging parameters on image artifacts and RF visibility. A virtual imaging platform has the potential to improve the understanding and use of CBCT technology, not only for researchers, but also for students, physicists, clinicians, and technologists. It is believed that improved insight into the system performance could lead to optimized imaging protocols, and can therefore help to reduce the large variation in system setup and performance currently seen in clinical practice.

ACKNOWLEDGMENTS

This work was supported by the Internal research fund of the Katholieke Universiteit Leuven (grant number C24/18/065). The computational resources and services used in this work were provided by the VSC (Flemish Supercomputer Center), funded by the Research Foundation Flanders (FWO) and the Flemish Government.

CONFLICTS OF INTEREST STATEMENT

The authors have no conflicts of interest to disclose.

REFERENCES

1. Brasil DM, Merken K, Binst J, Bosmans H, Haiter-Neto F, Jacobs R. Monitoring cone-beam CT radiation dose levels in a University Hospital. *Dentomaxillofac Radiol*. 2023;52:1-11.
2. Gaêta-Araujo H, Alzoubi T, Faria Vasconcelos K, et al. Cone beam computed tomography in dentomaxillofacial radiology: a two-decade overview. *Dentomaxillofa Radiol*. 2020;49:20200145.
3. Gaêta-Araujo H, Leite AF, Faria Vasconcelos K, Jacobs R. Two decades of research on CBCT imaging in DMFR - an appraisal of scientific evidence. *Dentomaxillofa Radiol*. 2021;49:20200367.
4. Merken K, Monnens J, Marshall N, et al. Development and validation of a 3D anthropomorphic phantom for dental CBCT imaging research. *Med Phys*. 2023;50:6714-6736.
5. Stowe J, O'Halloran C, Photopoulos G, et al. CTSim: Changing teaching practice in radiography with simulation. *Radiography*. 2021;27:490-498.
6. Abadi E, Segars WP, Tsui BMW, et al. Virtual clinical trials in medical imaging: a review. *J Med Imaging*. 2020;7:1-40.
7. Talwar S, Utneja S, Nawal RR, Kaushik A, Srivastava D, Oberoy SS. Role of cone-beam computed tomography in diagnosis of vertical root fractures: a systematic review and meta-analysis. *J Endod*. 2016;42:12-24.
8. Pinto MGO, Rabelo KA, Sousa Melo SL, et al. Influence of exposure parameters on the detection of simulated root fractures in the presence of various intracanal materials. *Int Endod J*. 2017;50:586-594.
9. Xanthis CG, Aletras AH. coreMRI: a high-performance, publicly available MR simulation platform on the cloud. *PLOS ONE*. 2019;14:e0216594.
10. Chaka B, Hardy M. Computer based simulation in CT and MRI radiography education: current role and future opportunities. *Radiography*. 2021;27:733-739.
11. Gunn T, Rowntree P, Starkey D, Nissen L. The use of virtual reality computed tomography simulation within a medical imaging and a radiation therapy undergraduate programme. *J Med Radiat Sci*. 2021;68:28-36.
12. Stratis A, Touyz N, Zhang G, et al. Development of a paediatric head voxel model database for dosimetric applications. *Br J Radiol*. 2017;90:1-13.
13. Rollins JD, Collins JS, Holden KR. United States head circumference growth reference charts: Bbirth to 21 years. *J Pediatr*. 2010;156:907-913.
14. Merken K. *A simulation framework for quality assessment and optimization in dento-maxillofacial CBCT imaging*. PhD thesis. KU Leuven; 2024.
15. Sempau J, Badal A, Brualla L. A PENELOPE-based system for the automated Monte Carlo simulation of clinacs and voxelized geometries-application to far-from-axis fields. *Med Phys*. 2011;38:5887-5895.

16. ICRP. The 2007 recommendations of the International Commission on Radiological Protection. In: *Annals of the ICRP*. Vol. 103. ICRP Publication; 2007;37.
17. Tapiovaara M, Siiskonen T. *PCXMC - A PC-based Monte Carlo Program for Calculating Patient Doses in Medical X-ray Examinations*. 2nd ed. Technical Report; 2008.
18. Stratis A. *Customized Monte Carlo modelling for paediatric patient dosimetry in dental and maxillofacial cone beam CT imaging*. PhD thesis. KU Leuven; 2018.
19. ICRP. Conversion coefficients for radiological protection quantities for external radiation exposures: ICRP publication 116. *Ann ICRP*. 2010;40:1-257.
20. ICRP,. Adult reference computational phantoms: ICRP publication 110. *Ann ICRP*. 2009;39:1-166.
21. Santos WS, Belinato W, Perini AP, et al. Occupational exposures during abdominal fluoroscopically guided interventional procedures for different patient sizes - a Monte Carlo approach. *Physica Med*. 2018;45:35-43.
22. Massera RT, Bosmans H, Rodriguez Perez S, Marshall N. A combined analytical and Monte Carlo method for detailed simulations of antiscatter grids in x-ray medical imaging: implementing scatter within the grid. *Phys Med Biol*. 2024;69:1-29.
23. Bueno MR, Azevedo BC, Estrela C. A critical review of the differential diagnosis of root fracture line in CBCT scans. *Braz Dent J*. 2021;32:114-128.
24. Gaêta-Araujo H, Souza G, Queiroz Freitas D, Oliveira-santos C. Optimization of tube current in cone-beam computed tomography for the detection of vertical root fractures with different intracanal materials. *J Endod*. 2017;43:1668-1673.
25. Guazzo R, Gardin C, Bellin G, et al. Graphene-based nanomaterials for tissue engineering in the dental field. *Nanomaterials*. 2018;8:349.
26. Nejaim Y, Farias Gomes A, Mazucatto Queiroz P, et al. Artifact expression of polylactic acid/hydroxyapatite/graphene oxide nanocomposite in CBCT: a promising dental material. *Clin Oral Investig*. 2020;24:1695-1700.
27. Sun T, Jacobs R, Pauwels R, Tijskens E, Fulton R, Nuyts J. A motion correction approach for oral and maxillofacial cone-beam CT imaging. *Phys Med Biol*. 2021;66:1-17.
28. Spin-Neto R, Wenzel A. Patient movement and motion artefacts in cone beam computed tomography of the dentomaxillofacial region: a systematic literature review. *Oral Surg Oral Med Oral Pathol Oral Radiol*. 2016;121:425-433.
29. Hegazy MAA, Cho MH, Cho MH, Lee SY. Metal artifact reduction in dental CBCT images using direct sinogram correction combined with metal path-length weighting. *Sensors*. 2023;23:1-15.
30. Park HS, Seo JK, Hyun CM, Lee SM, Jeon K. A fidelity-embedded learning for metal artifact reduction in dental CBCT. *Med Phys*. 2022;49:5195-5205.
31. Bayaraa T, Hyun CM, Jang TJ, Lee SM, Seo JK. A two-stage approach for beam hardening artifact reduction in low-dose dental CBCT. *IEEE Access*. 2020;8:225981-225994.
32. Kalender WA, Hebel R, Ebersberger J. Reduction of CT artifacts caused by metallic implants. *Radiology*. 1987;164:576-577.
33. Marinho Vieira LE, Lima E, Peixoto LR, et al. Assessment of the influence of different intracanal materials on the detection of root fracture in birooted teeth by cone-beam computed tomography. *J Endod*. 2020;46:264-270.
34. Rezende Barbosa GL, Sousa Melo SL, Alencar PNB, Nascimento MCC, Almeida SM. Performance of an artefact reduction algorithm in the diagnosis of in vitro vertical root fracture in four different root filling conditions on CBCT images. *Int Endod J*. 2016;49:500-508.
35. Freitas DQ, Vasconcelos TV, Noujeim M. Diagnosis of vertical root fracture in teeth close and distant to implant: an in vitro study to assess the influence of artifacts produced in cone beam computed tomography. *Clin Oral Investig*. 2019;23:1263-1270.
36. Fontenele RC, Gomes AF, Nejaim Y, Freitas DQ. Do the tube current and metal artifact reduction influence the diagnosis of vertical root fracture in a tooth positioned in the vicinity of a zirconium implant? a CBCT study. *Clin Oral Investig*. 2021;25:2229-2235.
37. Meyer E, Raupach R, Lell M, Schmidt B, Kachelrieß M. Normalized metal artifact reduction (NMAR) in computed tomography. *Med Phys*. 2010;37:5482-5493.
38. Meyer E, Raupach R, Lell M, Schmidt B, Kachelrieß M. Frequency split metal artifact reduction (FSMAR) in computed tomography. *Med Phys*. 2012;39:1904-1916.

How to cite this article: Merken K, Marshall N, Nuyts J, Massera RT, Jacobs R, Bosmans H. Demonstration of virtual imaging trial applications for optimization and education of dento-maxillofacial CBCT imaging. *Med Phys*. 2025;52:3487–3497.
https://doi.org/10.1002/mp.17708